Hindawi
Advances in Materials Science and Engineering
Volume 2018, Article ID 9014975, 8 pages
https://doi.org/10.1155/2018/9014975

*Research Article*

# High-Temperature Low-Cycle Fatigue Behaviour of MAR-M247 Coated with Newly Developed Thermal and Environmental Barrier Coating

**Ivo Šulák**,[1] **Karel Obrtlík**,[1] **Ladislav Čelko**,[2] **Pavel Gejdoš**,[2] **and David Jech**[2]

[1]*Institute of Physics of Materials, Academy of Sciences of the Czech Republic, Žižkova 22, 616 62 Brno, Czech Republic*
[2]*CEITEC–Central European Institute of Technology, Brno University of Technology, Purkyňova 123, 612 00 Brno, Czech Republic*

Correspondence should be addressed to Ivo Šulák; sulak@ipm.cz

Received 27 July 2018; Revised 16 November 2018; Accepted 9 December 2018; Published 24 December 2018

Academic Editor: Zhonghua Yao



This study investigates the strain-controlled low-cycle fatigue (LCF) behaviour of an untreated and surface-treated MAR-M247 superalloy in a symmetrical push-pull cycle with a constant strain rate at 900°C in laboratory air. A newly developed experimental thermal and environmental barrier coating (TEBC) system, consisting of a 170 $\mu$m thick CoNiCrAlY bond coat (BC) and a bilayer ceramic top coat (TC), with an interlayer and an upper layer, was deposited using air plasma spray techniques. The ceramic interlayer with an average thickness of 77 $\mu$m was formed from agglomerated and sintered yttria-stabilized zirconia. An experimental mixture of mullite ($Al_6Si_2O_{13}$) and hexacelsian ($BaAl_2Si_2O_8$) at a ratio of 70/30 vol.% was sprayed as the upper layer. The average thickness of the TC was 244 $\mu$m. The specimen sections were investigated using a TESCAN Lyra3 XMU scanning electron microscope (SEM) to characterise the microstructure of both the TEBC and the substrate material. The fatigue damage mechanisms in the TEBC-coated superalloy were studied. The fatigue life curves in the representation of the total strain amplitude versus the number of cycles to failure of the TEBC-coated and uncoated superalloy were assessed. TEBC was found to have a slight, positive effect on the fatigue life of MAR-M247.

## 1. Introduction

The inlet gas temperature in the hot section of high-temperature facilities often exceeds 1500°C (1200°C in contact with a component's surface), and the materials that are currently used, particularly superalloys, almost reach their temperature limits [1]. Moreover, the surface of the components is exposed to challenging environments in the hot section of gas turbines, and it has to be protected using different types of coatings [2]. Thermal barrier coatings (TBCs) protect metallic components from harsh environments and high temperatures in the hot section of turbine engines [2–4]. They are drafted on a dual layer system that consists of a metallic (CoNiCrAlY, NiCoCrAlY, and aluminium diffusion coatings) bond coat (BC) and a ceramic top coat (TC), mostly based on partially yttria-stabilized zirconia (YSZ). To date, YSZ has been widely used in many high-temperature facilities as the best solution for TC in TBC systems due to its suitable mechanical and thermal properties. Nonetheless, the call for high-performance aeroengines with increased resistance to a harsh environment has brought new challenges. The currently used YSZ coatings are susceptible to damage under service conditions due to environmental contaminants [5, 6]. The gathering of molten calcium-magnesium-aluminium-silicon (CMAS) oxide deposits on the surface is the main factor limiting the service life of YSZ, and recently, the process of infiltrating a molten CMAS deposit inside TBC coatings and its mitigation has attracted attention [5–10]. Pujol et al. [5] used a step-by-step methodology to investigate the interaction between YSZ aerogel powder and CMAS. They found that the X-ray diffraction (XRD) patterns of the YSZ contaminated by CMAS contain the diffraction peaks corresponding to the initial tetragonal YSZ as well as the monoclinic structure. This finding suggests that the tetragonal to monoclinic transformation occurred during the interaction

process via a dissolution/reprecipitation mechanism [5, 11]. The phase instability of the YSZ TC can lead to progressive cracking and delamination during service and cause overheating and early degradation of the superalloy with fatal consequences. Thus, current research is focused on the development and design of advanced CMAS-resistant thermal and environmental barrier coating (TEBC) systems with an enhanced thermal cycling lifetime and outstanding mechanical properties [12–16]. Čelko et al. [13] used solid-state synthesis to develop an experimental barium-magnesium-aluminium-silicate (BMAS) powder that was sprayed onto a MAR-M247 superalloy substrate in fully crystalline and partially amorphous conditions. The samples were subjected to a burner-rig test, and it was found that the BMAS coating in the fully crystalline condition was more durable than the partially amorphous one. However, under service conditions, the damage caused by the environment and high temperatures is in synergy with repeated elastic-plastic loading that represents fatigue damage. The effect of these coatings on the fatigue endurance of nickel-based superalloys has not been fully investigated. Recently, Obrtlík et al. [17] reported on the fatigue behaviour of a first-generation nickel-based superalloy coated with non-traditional oxidic TBCs. The study has shown that non-traditional oxidic TBCs have promising potential in relation to fatigue behaviour of nickel-based superalloys. Moreover, a combination of YSZ with near eutectic $ZrO_2$ + $SiO_2$ + $Al_2O_3$ has been found to provide the TC with sufficient cohesiveness and resistance to premature cracking during high-temperature mechanical loading [18].

The present study reports on the effect of a novel multilayer thermal and environmental barrier coating (TEBC) system on the fatigue behaviour of cast polycrystalline MAR-M247 at 900°C. Fatigue data of MAR-M247 have been reported under a wide range of loading conditions and temperatures [19–25]. The TBC consists of a metallic CoNiCrAlY BC and a bilayer ceramic TC made of a YSZ interlayer and a mullite ($Al_6Si_2O_{13}$) and hexacelsian ($BaAl_2Si_2O_8$) upper layer. The fatigue life curves in the total strain representation were obtained. The degradation mechanisms of the TBC-coated and uncoated material were investigated in specimen sections by means of scanning electron microscopy (SEM).

## 2. Materials and Methods

The MAR-M247 superalloy was produced as investment-cast cylindrical rods with dimensions close to the dimensions of the final specimen. Cylindrical specimens were machined from these rods to a final shape with a gauge length of 15 mm and a diameter of 6 mm. The nominal chemical composition of MAR-M247 is C (0.15 wt.%), Cr (8.37 wt.%), Co (9.91 wt.%), W (9.92 wt.%), Mo (0.67 wt.%), Al (5.42 wt.%), Ta (3.05 wt.%), Ti (1.01 wt.%), Fe (0.04 wt.%), Mn (<0.02 wt.%), Si (<0.03 wt.%), B (<0.015 wt.%), P (0.001 wt.%), S (0.001 wt.%), and Ni (balance). Polished and etched sections revealed dendritic grains with carbides, which were distributed in the interdendritic areas and at the grain boundaries. The number and size of the casting defects were reduced using hot isostatic pressing (100 MPa/1200°C/4 h). The optimal microstructure was achieved by heat treatment consisting of solid solution annealing (1200°C/24 h) and precipitation hardening (870°C/27 h). This microstructure contains $\gamma'$ precipitates coherently merged in a face-centred cubic (fcc) $\gamma$ matrix [19]. The average grain size was 2.3 ± 0.4 mm.

The TEBC coating was applied to a selected group of specimens. The deposition of the CoNiCrAlY BC via atmospheric plasma spraying (APS) using an F4MB-XL gun (Sulzer Metco, Pfäffikon, Switzerland) mounted on the 6-axis ABB industrial robot MF-P-1000 was done on a roughened surface prepared by grit blasting using pure 1 mm alumina particles. Two passes of a plasma gun were used to reduce the internal stresses within the BC. Commercially available powder (H. C. Starck Amperit 415, Goslar, Germany) with an average powder particle size of 45 ± 22 $\mu$m was used for the BC deposition. The multilayered ceramic TC was produced via APS under the same conditions as the BC deposition. The ceramic interlayer was formed from agglomerated and sintered YSZ powder (H. C. Stark Amperit 827, Goslar, Germany) with a particle size of 45 ± 10 $\mu$m. An experimental mixture of mullite ($Al_6Si_2O_{13}$) and hexacelsian ($BaAl_2Si_2O_8$) at the ratio of 70/30 vol.% was deposited as an upper layer. Based on the oxides present in the experimental TEBC mixture, this TEBC belongs to the family of the so-called BMAS coatings.

Low-cycle fatigue (LCF) tests were conducted on 10 uncoated specimens and 10 TEBC-coated specimens. A symmetrical push-pull cycle under strain control ($R_\varepsilon = -1$) was applied in a computer-controlled electrohydraulic testing system (MTS 810) at 900°C in laboratory air. The total strain amplitude and the strain rate ($\dot{\varepsilon} = 2 \times 10^{-3} \cdot s^{-1}$) were kept constant for all the tests. A closed three-zone resistance furnace was used to heat the specimens to 900°C. The temperature was monitored using three thermocouples attached to both ends of the specimens and to the upper part of the gauge length. Temperature gradient within the gauge length of the specimen at 900°C was ±1.5°C. Heating and cooling rate was set to be 300°C/hour in order to minimise damage of TEBC caused by thermal stresses originated from different coefficients of thermal expansion (CTE). The hysteresis loops for the selected number of cycles were recorded, and data were used for plastic strain amplitude analysis. Further experimental details regarding experimental setup and data analysis can be found elsewhere [17].

After LCF tests, the fracture surfaces and the polished sections parallel to the specimen axis were investigated using an Olympus DSX 510 optical microscope (OM) and a TESCAN Lyra3 XMU SEM to study the degradation processes in the TEBC-coated and uncoated superalloy. The chemical composition of the coating was investigated using an energy dispersive X-ray (EDX) spectroscopy analyser built into the SEM. The TEBC thickness and porosity measurements were obtained using image analysis Olympus Stream Enterprise Desktop 2.1 software. Details about the coating characterisation and methodology are reported in [17].

## 3. Results and Discussion

*3.1. Initial Microstructure.* The wide-field backscattered electron (BSE) image of the specimen section, presented in Figure 1, shows the initial microstructure of the TEBC system deposited onto the MAR-M247 superalloy substrate. Three distinguished areas can be recognised in the pristine microstructure of TEBC. From upside down, the experimental system consists of a mullite ($Al_6Si_2O_{13}$) (dark grey splats) and hexacelsian ($BaAl_2Si_2O_8$) (light grey splats) ceramic upper layer, as indicated in a detailed view in an inlet (a). The surface of the upper layer demonstrates that the upper layer coating is substantially nonuniform. The splats are irregularly shaped, and the feedstock powder ratio of 70/30 vol.% remained unchanged after the APS deposition. The hexacelsian splats are evenly distributed in the predominant mullite splats. Occasionally, thin cracks parallel to the specimen axis are present in the upper layer. The average thickness and porosity of this layer are 247 $\mu$m ± 21 $\mu$m and 5.45%, respectively. The YSZ ceramic interlayer is beneath this upper layer; it has an average thickness and porosity of 109 $\mu$m ± 10 $\mu$m and 9.13%, respectively. An inlet (c) shows the microcracks and cleavage defects present in the YSZ interlayer. The upper layer, together with the YSZ interlayer, forms an insulating TC system. The mullite + hexacelsian/YSZ interface is rough and free of defects (inlet (b)). Next, a CoNiCrAlY metallic BC was deposited onto the MAR-M247 substrate. The average thickness of BC was set to be 170 $\mu$m ± 12 $\mu$m. An inlet (e) shows the microstructure of the BC at a higher magnification. The phase composition of the metallic BC corresponds to the $\beta$ phase (NiAl) and the $\gamma/\gamma'$ phases. As seen in inlet (d), the YSZ/BC interface exhibits waviness and follows the surface of the grit-blasted substrate. The initial YSZ/BC interface does not contain a thermally grown oxide (TGO) scale layer. The interface between the BC and the superalloy is very rugged. Grit blasting was used to achieve the necessary mechanical bonding between the coatings and the substrate. Relict grit particles (inlet (f)) remain stuck in the MAR-M247 substrate. It has been reported that these particles can affect fatigue crack initiation and lifetime of material [26, 27]. Grit blasting also introduces compressive stresses that can decelerate the fatigue crack initiation and improve fatigue life [28, 29]. However, Šulák et al. [26] found that grit blasting has no effect on the lifetime of Inconel 713LC in the LCF region at 900°C. Due to grit blasting, the subsurface microstructure of MAR-M247 is heavily deformed. On average, the thickness of the deformed zone is 14 $\mu$m. The EDX maps of the plasma-sprayed TEBC presented in Figure 2 show the distribution of the elements in the mullite + hexacelsian and YSZ ceramic layers.

Figure 3 depicts the morphology of the surface of the TEBC-coated specimen in as-coated conditions and after a heating and cooling cycle. It can be seen that the as-coated TEBC surface is very rough with only a few capillary cracks or defects (Figure 3(a)) that could originate from a rapid cooling during a coating deposition process. The heating and cooling cycle consisting of heating to 900°C, 12 hours dwell and subsequent cooling to room temperature, was performed in order to test the thermal stability of TEBC. The heating and cooling rate was 600°C/hour. Figure 3(b) presents the BSE image of surface after the heating and cooling cycle. This heating and cooling cycle resulted in a prolongation of already existing cracks as well as an increased number of these cracks can be seen in detail in Figure 3(c). Metallographic section (Figure 3(d)) illustrates a capillary crack in the specimen after the heating and cooling cycle. The presence of these cracks could facilitate the fatigue crack initiation from the surface of the TC [17]. The YSZ interlayer as well as the mullite + hexacelsian/YSZ interface remained unaffected by the heating and cooling cycle. After 12 hour dwell at 900°C, a 1.04 ± 0.37 $\mu$m thick TGO scale was formed at the YSZ/BC interface. The TGO thickness after the heating and cooling cycle was not thick enough to cause delamination of the TC [30].

*3.2. Degradation of TEBC under Fatigue Loading.* A number of capillary cracks that are present in the TEBC coating after deposition in a combination with natural brittleness of ceramic coatings can facilitate the surface fatigue crack initiation in the TEBC-coated specimens [17, 31]. Post-experimental observation of the specimen section revealed the degradation of the TEBC system during cyclic loading at 900°C. Both, surface and subsurface fatigue crack initiation was observed. The fatigue cracks that nucleated at the TEBC surface and subsequently penetrated through the TEBC to the substrate are shown in Figure 4(a). A number of short fatigue cracks can be found within the upper layer after fatigue loading, as shown in Figure 4(b). Initiation and propagation of the fatigue cracks are independent of the splat boundaries. Surface crack initiation is also a decisive mechanism in the uncoated MAR-M247 [23]. The crack growth paths are predominantly oriented perpendicularly to the loading axis. Some of the cracks changed their path and became almost parallel with the loading axis. The number of capillary cracks in the YSZ interlayer was very low, which can be attributed to better strain tolerance in the YSZ interlayer in comparison to the upper layer. Typical delamination was observed primarily in the upper layer close to the mullite + hexacelsian/YSZ interface, as can be seen in Figure 4(c). The mullite + hexacelsian/YSZ interface is free of any defects or newly formed phases. In the LCF tests with total strain amplitudes higher than $\varepsilon_a$ = 0.30%, the delamination of the YSZ interlayer was observed approximately 15–30 $\mu$m far from the YSZ/BC interface (Figure 4(a)). The LCF tests with lower strain amplitudes showed that the YSZ interlayer stayed attached to the BC without macroscopically perceptible delamination (Figure 4(c)). However, detailed inspection of the YSZ/BC interface revealed occasional local delamination of the YSZ interlayer in the vicinity of the secondary fatigue cracks (Figure 4(d)). Hutařová et al. [32] reported on the degradation of the YSZ-coated Inconel 713LC. The fatigue crack initiation was found usually at the YSZ/BC interface of the YSZ-coated Inconel 713LC. In the present work, fatigue crack initiation at the YSZ/BC interface TEBC-coated MAR-M247 was also occasionally identified (Figure 4(d)). TGOs formation was found at the TC/BC interface and at the newly

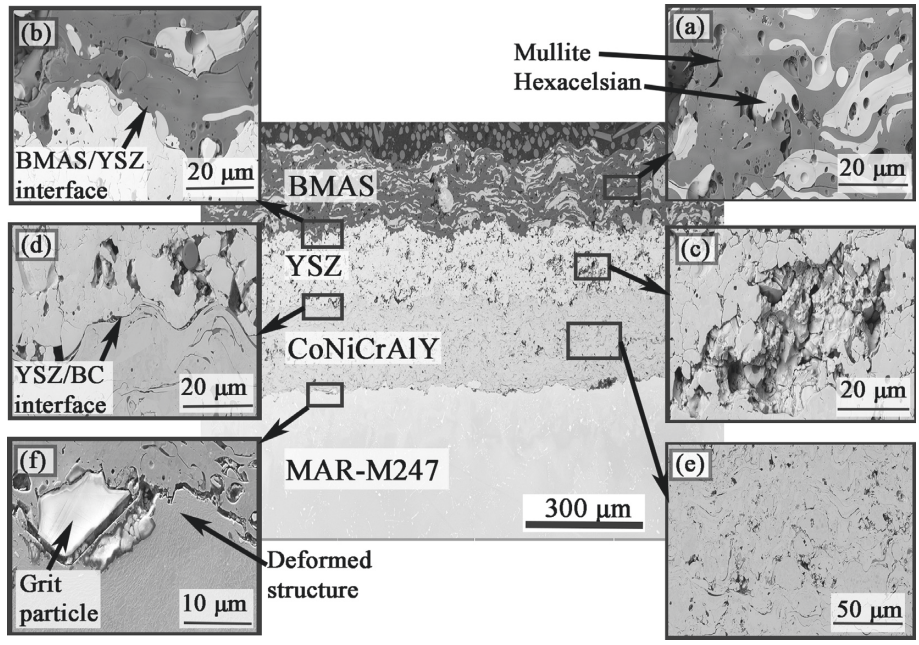


Figure 1: The microstructure of the TEBC system deposited onto the MAR-M247 superalloy substrate. List of insets: (a) detail of the mullite + hexacelsian upper layer; (b) the mullite + hexacelsian/YSZ interface; (c) detail of the YSZ interlayer; (d) the YSZ/BC interface; (e) the CoNiCrAlY BC; (f) the BC/MAR-M247 interface with $Al_2O_3$ grit particle.

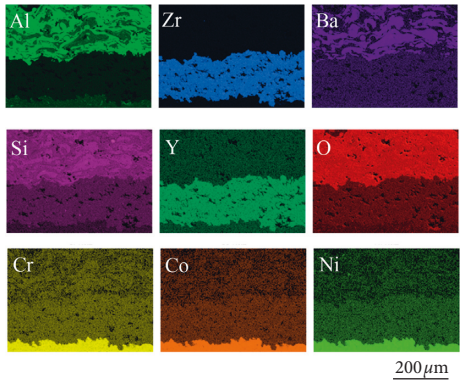


Figure 2: EDX elemental maps of TEBC showing distribution of the main elements presented in the TC and BC: (a) Al; (b) Zr; (c) Ba; (d) Si; (e) Y; (f) O; (g) Cr; (h) Co; (i) Ni.

formed surfaces of the fatigue cracks that occurred during LCF loading at 900°C. This can be explained as a consequence of oxygen access through the pores and capillary cracks that are naturally present in the TC between individual splats. The thickness of the TGO at the TC/BC interface varied from 1.25 ± 0.43 $\mu$m to 2.56 ± 0.51 $\mu$m with the test duration ranging from 12 h to 58 h, respectively. Figure 4(d) shows the TGO scale in the specimen exposed to 900°C for 58 h ($\varepsilon_a$ = 0.15%). The YSZ/CoNiCrAlY interface is a significant crack initiation source in specimens that are exposed to 900°C longer than 36 h. As the oxidation proceeds and the TGO scale reaches critical thickness, it is probable that the cracks at the YSZ/CoNiCrAlY interface would be initiated by an increase in the local stresses [33–35]. Similarly to our previous studies [17, 36], fatigue crack initiation at BC/substrate interface was identified in the vicinity of embedded grit particles (Figure 4(a)). It was proven by Warnes et al. [27] that elimination of these particles can improve fatigue life of coated MAR-M247 under thermo-mechanical loading by 40%.

*3.3. Fracture Surface.* The SEM micrograph of a fracture surface of the TEBC-coated specimen cycled with total strain amplitude equal to 0.38% is shown in Figure 5(a). The fatigue crack propagates from the specimen surface through the TC and the BC to the substrate. The transgranular crack growth path is visible in the middle of the image. A detail of area (b) is shown in Figure 5(b), and it presents the cleavage fracture of the upper layer of the TEBC. Hexacelsian splats are typical of short facets, whereas mullite splats exhibit longer facets. Moreover, small pores are present in the mullite phase. Cleavage fracture can be seen in the YSZ interlayer as well (Figure 5(c)). The brittle behaviour suggests that the TC could be damaged in the very beginning of fatigue life, and only the substrate and the BC are involved in the fatigue loading transfer. In this particular type of loading, the TC may only provide environmental protection; its mechanical contribution would be insignificant.

*3.4. Fatigue Life.* Figure 6 shows the fatigue life diagram in the representation of the total strain amplitude $\varepsilon_a$ versus the number of cycles to failure $N_f$ of both the TEBC-coated MAR-M247 and the uncoated MAR-M247. The results show that TEBC can slightly increase the fatigue life of MAR-M247. In general, application of TBC leads to a reduction of fatigue life [37–40]. An increase in fatigue lifetime by this particular TEBC is very important for its industrial application. Factors that contribute to the higher fatigue life of

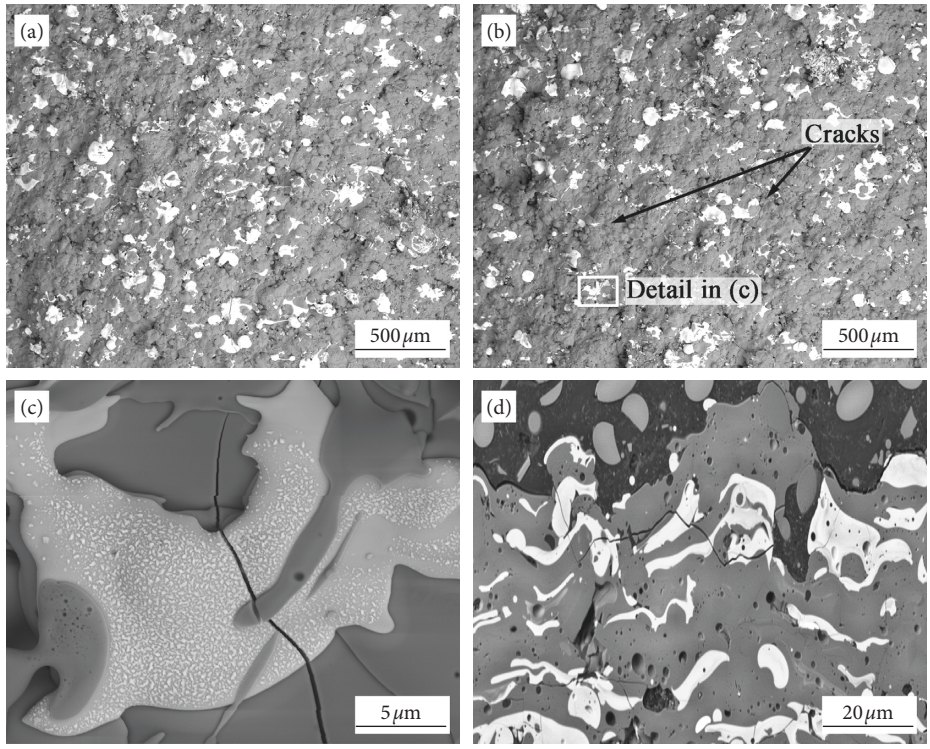


Figure 3: Surface morphology of TEBC coating in (a) as-coated conditions, (b) after the heating and cooling cycle, and (c, d) detail showing cracks after heating and cooling cycle.

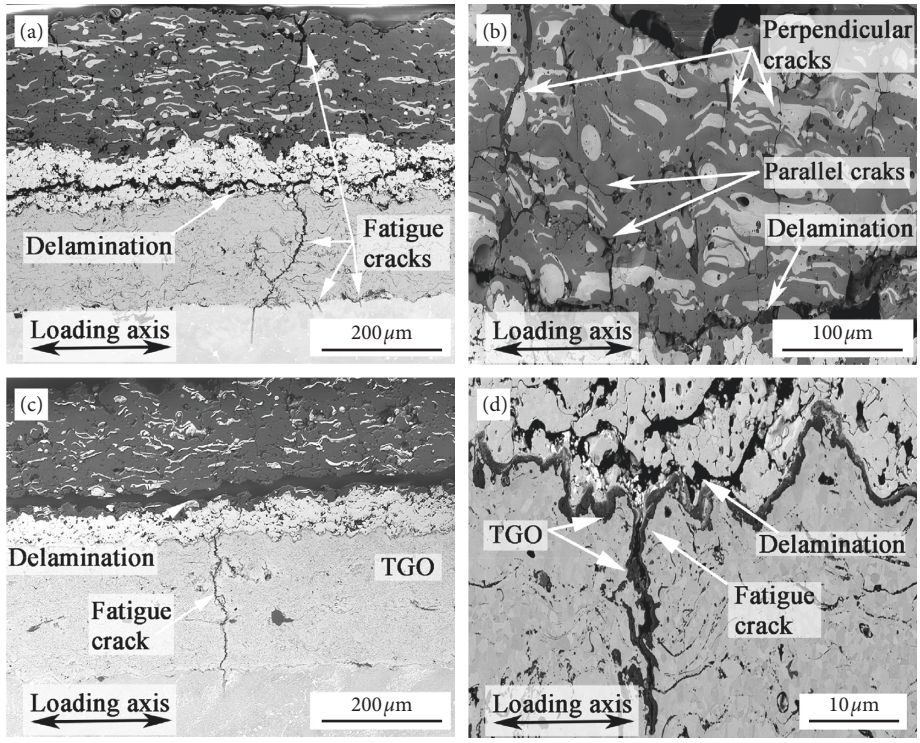


Figure 4: Degradation of the TEBC system. (a) Delamination of YSZ, $\varepsilon_a = 0.30\%$; (b) fatigue cracking and delamination of the mullite + hexacelsian upper layer, $\varepsilon_a = 0.30\%$; (c) degradation of TEBC after LCF, $\varepsilon_a = 0.15\%$; (d) TGO scale at the YSZ/CoNiCrAlY interface, $\varepsilon_a = 0.30\%$.

TEBC-coated MAR-M247 are (i) increased number of cracks in the TEBC-coated material in comparison with uncoated MAR-M247. This suppresses the localization of the plastic strain, and thus, the fatigue crack initiation and propagation can be longer [36, 41]; (ii) corrosion and oxidation protection of materials that are employed in harsh

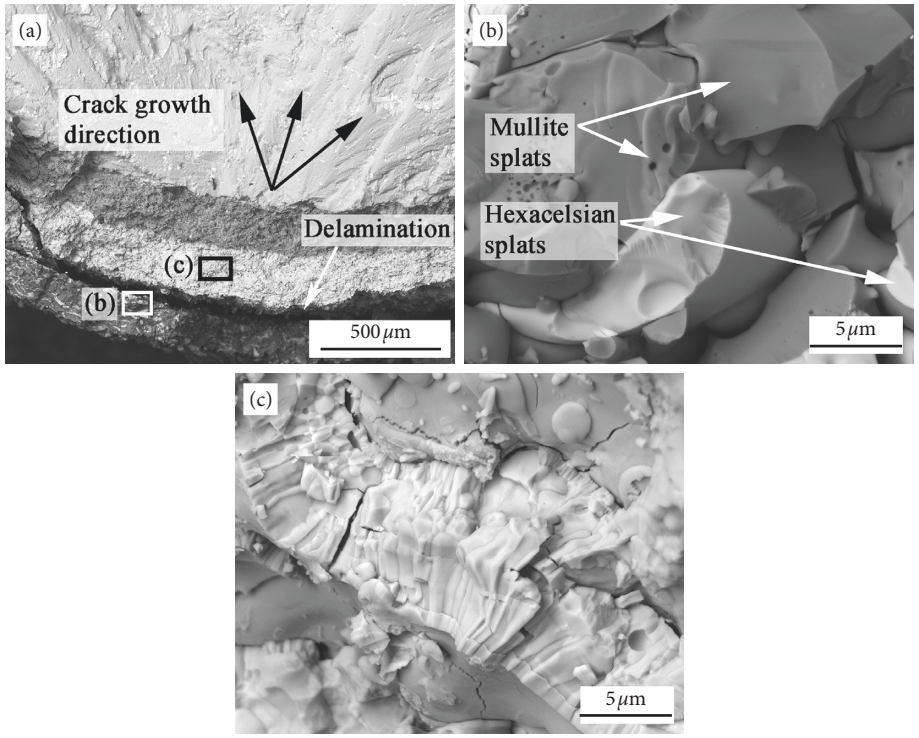


FIGURE 5: Fracture surface of the specimen fatigued to failure, $\varepsilon_a$ = 0.38%: (a) surface initiation site and crack growth path; (b) cleavage fracture of the upper layer splats; (c) cleavage fracture of the YSZ splats.

environments is very important. However, corrosion and oxidation resistance of MAR-M247 is comparatively poor due to the relatively low content of chromium, and the unprotected surface of uncoated MAR-M247 degrades quickly [42]. TEBCs were tailored to provide mainly thermal insulation, but their multilayer structure also provides outstanding oxidation and corrosion resistance and therefore fatigue life of TEBC-coated MAR-M247 is higher in comparison with uncoated MAR-M247. Yet, there exists a crossover when the strain amplitudes are ≤0.17%; then, the fatigue life of the TEBC-coated specimens is slightly shorter than the fatigue life of the uncoated specimens. To further interpret the fatigue behaviour of the TEBC-coated MAR-M247 and the uncoated MAR-M247, the data of plastic strain amplitude vs. total strain amplitude are plotted in Figure 7. It is a consensus that a higher plastic strain corresponds to a shorter fatigue life. However, Figure 7 shows that TEBC-coated MAR-M247 exhibits higher plastic strain amplitudes when the strain amplitudes are ≤0.25% and fatigue life in Figure 6 is lower for amplitudes ≤0.17%. This crossover mismatch in Figures 6 and 7 can originate from two completive factors (i) plastic strain amplitude and (ii) environmental protection of the material that is given by TEBC. The protective effect of the TEBC on the substrate at 900°C plays an important role in fatigue life, and it is mostly possible that the protective effect of TEBC is more beneficial than the effect of higher plastic strain amplitude. The existence of the crossover in Figure 7 could be explained by the different ratio of fatigue cracks that are present in the substrate of the TEBC-coated and uncoated material. The

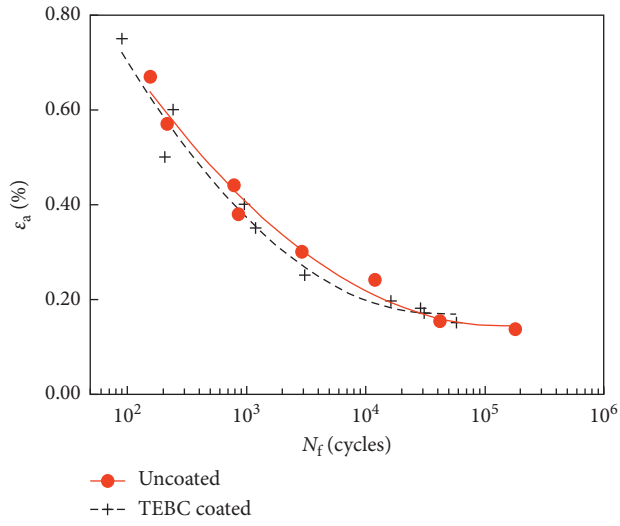


FIGURE 6: Fatigue life curves of TEBC-coated and uncoated MAR-M247 superalloy.

ratio increases with a decrease in the strain amplitude. The ratio (cracks that penetrate to the substrate-TEBC-coated to uncoated MAR-M247) of 2.18 and 6.3 corresponds to the highest and lowest strain amplitude, respectively [17, 36]. This suggests that, with a decrease in the strain amplitude, a comparatively higher crack density can result in the fatigue crack interaction in the short crack growth domain that accelerates the main crack formation and decreases the fatigue life [43].

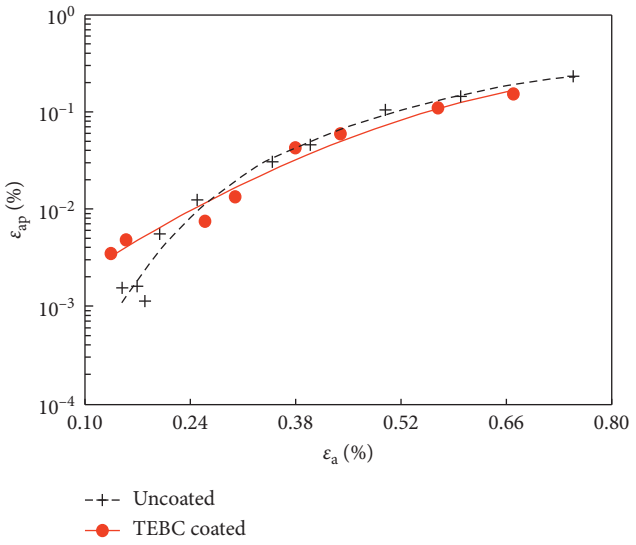


Figure 7: Plastic strain amplitude $\varepsilon_{ap}$ as a function of total strain amplitude $\varepsilon_a$.

## 4. Summary and Conclusions

The following summary and conclusions can be drawn from this study, which investigated the effect of TEBC, consisting of a mullite + hexacelsian upper layer, a YSZ interlayer, and a CoNiCrAlY BC, on the high-temperature LCF behaviour of MAR-M247.

(1) A thin subsurface layer of the MAR-M247 substrate is deformed as a result of grit blasting. Some of the $Al_2O_3$ grit particles remain embedded in the substrate.

(2) The TGO scale is not present at the initial YSZ/CoNiCrAlY interface. The thickness of the TGO scale increases with the duration of the LCF test. As soon as the TGO scale reaches critical thickness, YSZ delamination and cracking are facilitated.

(3) Fatigue cracks mainly initiate in the upper layer and, to a lesser extent, from the new surfaces, as a result of ceramic layer delamination and the presence of grit particles.

(4) The cleavage nature of the fracture in the mullite + hexacelsian and YSZ layers was identified.

(5) TEBC was found to have a slight, positive effect on the fatigue life of MAR-M247 in the representation of the total strain amplitude vs. the number of cycles to failure.

## Data Availability

The .XLSX, .DBF, .ALF, and .RAW data used to support the findings of this study are available from the corresponding author upon request.

## Conflicts of Interest

The authors declare that there are no conflicts of interest regarding the publication of this paper.

## Acknowledgments

The present research was conducted under the support of project IPMinfra, LM2015069.

## References

[1] R. C. Reed, *The Superalloys: Fundamentals and Applications*, Cambridge University Press, Cambridge, UK, 1st edition, 2008.

[2] S. Bose, *High Temperature Coatings*, Butterworth-Heinemann, Burlington, NJ, USA, 2007.

[3] S. Tailor, R. M. Mohanty, and A. V. Doub, "Development of a new TBC system for more efficient gas turbine engine application," *Materials Today: Proceedings*, vol. 3, no. 8, pp. 2725–2734, 2016.

[4] R. Vaßen, M. O. Jarligo, T. Steinke, D. E. Mack, and D. Stöver, "Overview on advanced thermal barrier coatings," *Surface and Coatings Technology*, vol. 205, no. 4, pp. 938–942, 2010.

[5] G. Pujol, F. Ansart, J.-P. Bonino, A. Malié, and S. Hamadi, "Step-by-step investigation of degradation mechanisms induced by CMAS attack on YSZ materials for TBC applications," *Surface and Coatings Technology*, vol. 237, pp. 71–78, 2013.

[6] C. G. Levi, J. W. Hutchinson, M.-H. Vidal-Sétif, and C. A. Johnson, "Environmental degradation of thermal-barrier coatings by molten deposits," *MRS Bulletin*, vol. 37, no. 10, pp. 932–941, 2012.

[7] H. Zhao, C. G. Levi, and H. N. G. Wadley, "Molten silicate interactions with thermal barrier coatings," *Surface and Coatings Technology*, vol. 251, pp. 74–86, 2014.

[8] R. W. Jackson, E. M. Zaleski, D. L. Poerschke, B. T. Hazel, M. R. Begley, and C. G. Levi, "Interaction of molten silicates with thermal barrier coatings under temperature gradients," *Acta Materialia*, vol. 89, pp. 396–407, 2015.

[9] M. H. Vidal-Setif, N. Chellah, C. Rio, C. Sanchez, and O. Lavigne, "Calcium-magnesium-alumino-silicate (CMAS) degradation of EB-PVD thermal barrier coatings: characterization of CMAS damage on ex-service high pressure blade TBCs," *Surface and Coatings Technology*, vol. 208, pp. 39–45, 2012.

[10] A. R. Krause, X. Li, and N. P. Padture, "Interaction between ceramic powder and molten calcia-magnesia-alumino-silicate (CMAS) glass, and its implication on CMAS-resistant thermal barrier coatings," *Scripta Materialia*, vol. 112, pp. 118–122, 2016.

[11] S. Krämer, J. Yang, C. G. Levi, and C. A. Johnson, "Thermochemical interaction of thermal barrier coatings with molten CaO-MgO-$Al_2O_3$-$SiO_2$ (CMAS) deposits," *Journal of the American Ceramic Society*, vol. 89, no. 10, pp. 3167–3175, 2006.

[12] G. Di Girolamo and E. Serra, "Thermally sprayed nanostructured coatings for anti-wear and TBC applications: state-of-the-art and future perspectives," in *Anti-Abrasive Nanocoatings*, M. Aliofkhazraei, Ed., Woodhead Publishing, Sawston, UK, pp. 513–541, 2015.

[13] L. Čelko, D. Jech, K. Dvořák, I. Šulák, L. Klakurková, and K. Obrtlík, "Durability of amorphous and crystalline BMAS thermal barrier coatings produced by plasma spraying," *Solid State Phenomena*, vol. 258, pp. 383–386, 2017.

[14] B. Zhang, L. Wei, L. Gao, H. Guo, and H. Xu, "Microstructural characterization of PS-PVD ceramic thermal barrier coatings with quasi-columnar structures," *Surface and Coatings Technology*, vol. 311, pp. 199–205, 2017.

[15] A. K. Rai, R. S. Bhattacharya, D. E. Wolfe, and T. J. Eden, "CMAS-resistant thermal barrier coatings (TBC)," *International Journal of Applied Ceramic Technology*, vol. 7, no. 5, pp. 662–674, 2009.

[16] L. Wei, L. Guo, M. Li, and H. Guo, "Calcium-magnesium-alumina-silicate (CMAS) resistant $Ba_2REAlO_5$ (RE = Yb, Er, Dy) ceramics for thermal barrier coatings," *Journal of the European Ceramic Society*, vol. 37, no. 15, pp. 4991–5000, 2017.

[17] K. Obrtlík, L. Čelko, T. Chráska, I. Šulák, and P. Gejdoš, "Effect of alumina-silica-zirconia eutectic ceramic thermal barrier coating on the low cycle fatigue behaviour of cast polycrystalline nickel-based superalloy at 900°C," *Surface and Coatings Technology*, vol. 318, pp. 374–381, 2017.

[18] I. Šulák, K. Obrtlík, L. Čelko, and P. Gejdoš, "Degradation of YSZ/EUCOR TBC coating system during high temperature low cycle fatigue tests," *Solid State Phenomena*, vol. 258, pp. 420–423, 2017.

[19] I. Šulák, K. Obrtlík, and L. Čelko, "High-temperature low-cycle fatigue behaviour of HIP treated and untreated superalloy MAR-M247," *Metallic Materials*, vol. 54, no. 6, pp. 471–481, 2016.

[20] M. Šmíd, L. Kunz, P. Hutař, and K. Hrbáček, "High cycle fatigue of nickel-based superalloy MAR-M 247 at high temperatures," *Procedia Engineering*, vol. 74, pp. 329–332, 2014.

[21] M. Šmíd, V. Horník, P. Hutař, K. Hrbáček, and L. Kunz, "High cycle fatigue damage mechanisms of MAR-M 247 superalloy at high temperatures," *Transactions of the Indian Institute of Metals*, vol. 69, no. 2, pp. 393–397, 2016.

[22] I. Šulák and K. Obrtlík, "Fatigue crack initiation in nickel-based superalloy MAR-M247 at high temperature," *Key Engineering Materials*, vol. 754, pp. 27–30, 2017.

[23] I. Šulák and K. Obrtlík, "Effect of tensile dwell on high-temperature low-cycle fatigue and fracture behaviour of cast superalloy MAR-M247," *Engineering Fracture Mechanics*, vol. 185, pp. 92–100, 2017.

[24] D. A. Boismier and H. Sehitoglu, "Thermo-mechanical fatigue of Mar-M247: Part 1-experiments," *Journal of Engineering Materials and Technology*, vol. 112, no. 1, pp. 68–79, 1990.

[25] H. Sehitoglu and D. A. Boismier, "Thermo-mechanical fatigue of Mar-M247: Part 2-life prediction," *Journal of Engineering Materials and Technology*, vol. 112, no. 1, pp. 80–89, 1990.

[26] I. Šulák, K. Obrtlík, and L. Čelko, "High temperature low cycle fatigue characteristics of grit blasted polycrystalline Ni-base superalloy," *Key Engineering Materials*, vol. 665, pp. 73–76, 2016.

[27] B. M. Warnes, A. L. Purvis, and J. E. Schilbe, "The manufacture and fatigue cracking resistance of grit free aluminide diffusion coatings," *Surface and Coatings Technology*, vol. 163-164, pp. 100–105, 2003.

[28] K. Poorna Chander, M. Vashista, K. Sabiruddin, S. Paul, and P. P. Bandyopadhyay, "Effects of grit blasting on surface properties of steel substrates," *Materials & Design*, vol. 30, no. 8, pp. 2895–2902, 2009.

[29] T. Klotz, D. Delbergue, P. Bocher, M. Lévesque, and M. Brochu, "Surface characteristics and fatigue behavior of shot peened Inconel 718," *International Journal of Fatigue*, vol. 110, pp. 10–21, 2018.

[30] D. Jech, L. Čelko, T. Chráska et al., "Influence of isothermal exposure on microstructural changes resulting in delamination of eutectic $Al_2O_3$ + $ZrO_2$ +$SiO_2$ thermal barrier coatings," in *Proceedings of 23rd International Conference on Metallurgy and Materials*, Brno, Czech Republic, May 2014.

[31] T. Chráska, J. Hostomský, M. Klementová, and J. Dubský, "Crystallization kinetics of amorphous alumina-zirconia-silica ceramics," *Journal of the European Ceramic Society*, vol. 29, no. 15, pp. 3159–3165, 2009.

[32] S. Hutařová, K. Obrtlík, M. Juliš, L. Čelko, M. Hrčková, and T. Podrábský, "Degradation of TBC coating during low-cycle fatigue tests at high temperature," *Key Engineering Materials*, vol. 592-593, pp. 461–464, 2014.

[33] K. Slámečka, P. Skalka, J. Pokluda, and L. Čelko, "Finite element simulation of stresses in a plasma-sprayed thermal barrier coating with an irregular top-coat/bond-coat interface," *Surface and Coatings Technology*, vol. 304, pp. 574–583, 2016.

[34] P. Skalka, K. Slámečka, J. Pokluda, and L. Čelko, "Finite element simulation of stresses in a plasma-sprayed thermal barrier coating with a crack at the TGO/bond-coat interface," *Surface and Coatings Technology*, vol. 337, pp. 321–334, 2018.

[35] M. Jinnestrand and H. Brodin, "Crack initiation and propagation in air plasma sprayed thermal barrier coatings, testing and mathematical modelling of low cycle fatigue behaviour," *Materials Science and Engineering: A*, vol. 379, no. 1-2, pp. 45–57, 2004.

[36] I. Šulák, K. Obrtlík, L. Čelko, T. Chráska, D. Jech, and P. Gejdoš, "Low cycle fatigue performance of Ni-based superalloy coated with complex thermal barrier coating," *Materials Characterization*, vol. 139, pp. 347–354, 2018.

[37] K. Slámečka, L. Čelko, P. Skalka et al., "Bending fatigue failure of atmospheric-plasma-sprayed CoNiCrAlY + YSZ thermal barrier coatings," *International Journal of Fatigue*, vol. 70, pp. 186–195, 2015.

[38] R. Nutzel, E. Affeldt, and M. Göken, "Damage evolution during thermo-mechanical fatigue of a coated monocrystalline nickel-base superalloy," *International Journal of Fatigue*, vol. 30, no. 2, pp. 313–317, 2008.

[39] S. Kuba, Y. Kojima, and H. Suzuki, "Effect of thermal barrier coating layer on HIP treated IN738LC fatigue characteristic," *Key Engineering Materials*, vol. 306–308, pp. 109–114, 2006.

[40] K. Obrtlík, S. Hutařová, L. Čelko, M. Juliš, T. Podrábský, and I. Šulák, "Effect of thermal barrier coating on low cycle fatigue behavior of cast Inconel 713LC at 900°C," *Advanced Materials Research*, vol. 891-892, pp. 848–853, 2014.

[41] J. Pokluda and P. Šandera, *Micromechanisms of Fracture and Fatigue*, Springer London, London, UK, 2010.

[42] M. Kianicová, J. Kafrík, and J. Trník, "Degradation of aluminide coatings deposited on nickel superalloys," *Procedia Engineering*, vol. 136, pp. 346–352, 2016.

[43] A. Vašek, J. Polák, and K. Obrtlík, "Fatigue damage in two-step loading of 316l steel II. Short crack growth," *Fatigue & Fracture of Engineering Materials and Structures*, vol. 19, no. 2-3, pp. 157–163, 1996.